

## Pore Space Partition and Charge Separation in Cage-within-Cage Indium–Organic Frameworks with High CO<sub>2</sub> Uptake

Shou-Tian Zheng,<sup>†</sup> Julia T. Bu,<sup>‡,§</sup> Yufei Li,<sup>†</sup> Tao Wu,<sup>‡</sup> Fan Zuo,<sup>‡</sup> Pingyun Feng,<sup>\*,‡</sup> and Xianhui Bu<sup>\*,†</sup>

*Department of Chemistry and Biochemistry, California State University, Long Beach, California 90840, United States, and Department of Chemistry, University of California, Riverside, California 92521, United States*

Received August 2, 2010; E-mail: xbu@csulb.edu; pingyun.feng@ucr.edu

**Abstract:** The integration of negatively charged single-metal building blocks {In(CO<sub>2</sub>)<sub>4</sub>} and positively charged trimeric clusters {In<sub>3</sub>O} leads to three unique cage-within-cage-based porous materials, which exhibit not only high hydrothermal, thermal, and photochemical stability but also attractive structural features contributing to a very high CO<sub>2</sub> uptake capacity of up to 119.8 L/L at 273 K and 1 atm.

Crystalline porous materials are an important class of materials due to their large-scale industrial applications in heterogeneous catalysis, gas separation, and so on.<sup>1,2</sup> In recent years, there has been an intensive effort aimed at the design of new generations of porous materials that can be used as high-capacity adsorbents for gas storage and delivery or CO<sub>2</sub> sequestration.<sup>3–5</sup> Among many different types of materials studied for such purposes, metal–organic framework materials (MOFs) have emerged as one of the favorites because of their compositional and geometric tunability and very high surface areas.<sup>6,7</sup>

It has been recognized that high surface area and large pore volume do not necessarily lead to a high uptake capacity for small molecules such as CO<sub>2</sub>, especially under ambient conditions. Recent studies have indicated several features that are desirable for enhancing storage capacity of small gas molecules.<sup>8–10</sup> One such feature is the suitable pore size commensurate with the size of a gas molecule. This makes it necessary to develop synthetic strategies to generate a pore architecture that allows for efficient use of the pore space, for example, through pore space partitioning of large cage structures using methods such as impregnation and catenation. Another factor currently receiving considerable attention is the generation of individual localized binding sites using methods such as (1) creation of coordinatively unsaturated metal sites (also called open-metal sites) located on either inorganic nodes or organic linkers (or as extraframework species, like Li<sup>+</sup> in zeolite X) and (2) use of organic linkers with functional groups such as –NH<sub>2</sub>.<sup>4</sup> Furthermore, the solid–gas interactions can also be enhanced using a somewhat delocalized approach through the generation of the electric field across the pore space that is capable of polarizing gas molecules and increasing their interaction with charged internal pore surfaces or charged extraframework species.<sup>11</sup> However, this latter approach is far less well studied experimentally because the vast majority of MOFs have an electrically neutral framework.

Here we report three interesting cage-within-cage porous In–carboxylate frameworks [(CH<sub>3</sub>)<sub>2</sub>NH<sub>2</sub>][In<sub>3</sub>O(BTC)<sub>2</sub>(H<sub>2</sub>O)<sub>3</sub>]<sub>2</sub>–[In<sub>3</sub>(BTC)<sub>4</sub>]·7DMF·23H<sub>2</sub>O (denoted as CPM-5, CPM = crystalline

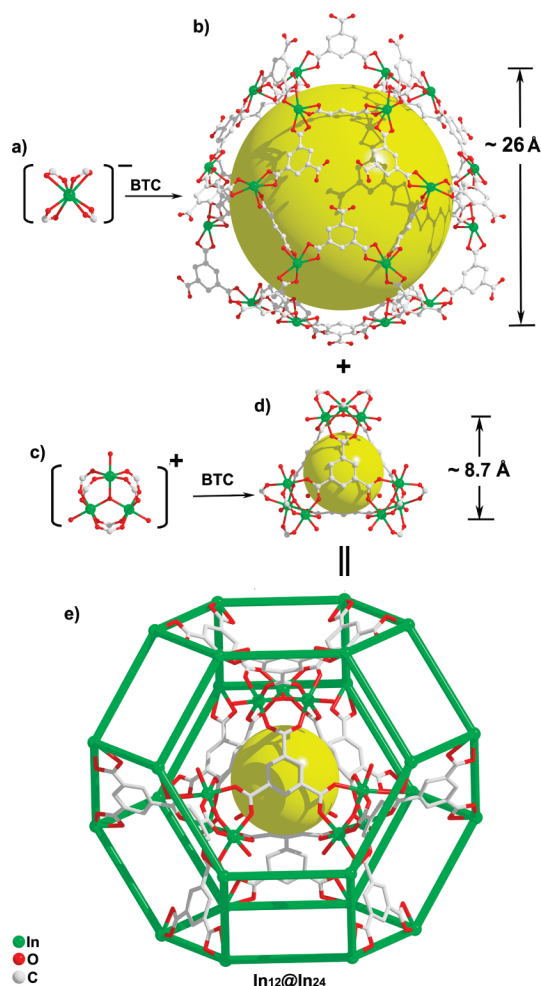


**Figure 1.** (a–e) Structures of monomeric In<sup>3+</sup> ion, In<sub>24</sub> cage, trimeric {(In<sub>3</sub>O)(H<sub>2</sub>O)<sub>3</sub>} unit, In<sub>12</sub> cage, and In<sub>12</sub>@In<sub>24</sub> cage, respectively. The green solid lines represent BTCs.

porous materials), [(CH<sub>3</sub>)<sub>2</sub>NH<sub>2</sub>][In<sub>3</sub>O(BTC)<sub>2</sub>(H<sub>2</sub>O)<sub>3</sub>]<sub>2</sub>[In(BTC)<sub>4/3</sub>][In(BTC)<sub>4/3</sub>(H<sub>2</sub>O)<sub>2</sub>]·solvent (CPM-5'), and [CH<sub>3</sub>NH<sub>3</sub>][In<sub>3</sub>O(BTC)<sub>2</sub>(H<sub>2</sub>O)<sub>3</sub>]<sub>2</sub>[In<sub>3</sub>(BTC)<sub>4</sub>]·solvent (CPM-6, BTC = 1,3,5-benzenetricarboxylate) that integrate several aforementioned features (e.g., pore size partition, charged frameworks, and open metal sites) and exhibit high CO<sub>2</sub> uptake capacity. CPM-5 crystallizes in a highly symmetric and yet noncentrosymmetric cubic space group  $\bar{I}43m$ . As shown in Figure 1e, its most fascinating topological feature is the cage-within-cage structure in which a large Archimedean cage (truncated octahedral cage, also called sodalite cage, denoted as the In<sub>24</sub> cage here) encapsulates a small Archimedean cage (truncated tetrahedral cage, denoted as the In<sub>12</sub> cage here). The outer sodalite cage is

<sup>†</sup> California State University, Long Beach.

<sup>‡</sup> University of California, Riverside.

<sup>§</sup> Research Intern from J. W. North High School, Riverside.

formed by 24 mononuclear  $\text{In}^{3+}$  sites, each of which is eight-coordinated to oxygen atoms, but serves as a four-connected node because of the formation of the chelate bond (Figure 1a). Any two adjacent  $\text{In}^{3+}$  sites on the  $\text{In}_{24}$  cage are bridged by a  $\text{BTC}^{3-}$  anion using two of its three carboxylic groups, forming a sodalite cage (Figure 1b) that is significantly larger than other MOFs with a sodalite topology such as ZIF-8 and sod-ZMOF (Table S1).<sup>6b,12</sup> The third carboxylic group of each BTC serves to interconnect the outer  $\text{In}_{24}$  cage with the inner  $\text{In}_{12}$  cage (Figure 1c).<sup>13a</sup> The  $\text{In}_{12}$  cage is built from four trimeric  $\{[\text{In}_3(\text{O})(\text{H}_2\text{O})_3]\}$  clusters which are joined together by four BTCs into a truncated tetrahedron  $\{[\text{In}_3(\text{H}_2\text{O})_3(\mu_3\text{-O})_4(\text{BTC})_4]\}$  (Figures 1c, 1d).

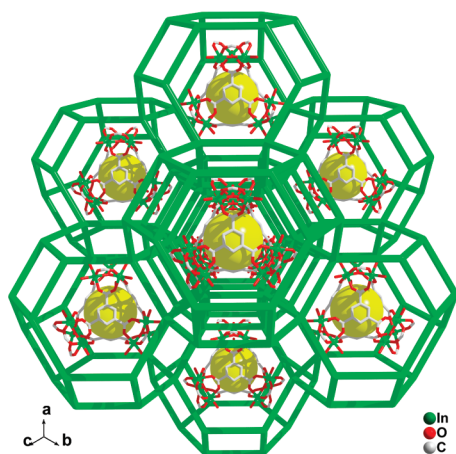


**Figure 2.** View of the 3D structure of CPM-5. Some BTC ligands interconnecting  $\text{In}_{12}$  and  $\text{In}_{24}$  cages are omitted for clarity.

The overall 3D structure can be understood as a body-centered cubic packing of the larger  $\text{In}_{24}$  cages, each of which contains one  $\text{In}_{12}$  cage at the center (Figure 2). Although a number of metal–organic polyhedral frameworks have been reported,<sup>13,14</sup> so far there are few examples of the cage-within-cage-based 3D polyhedral framework. The formation of the core–shell-type  $\text{In}_{12}@\text{In}_{24}$  3D structure has the potential to enhance sorption properties of small gas molecules such as  $\text{CO}_2$ . First, the  $\text{In}_{24}$  cage which is about  $25.7 \times 25.7 \times 25.7 \text{ \AA}^3$  in dimension is far too large for the storage of small gas molecules. The interconnection between the  $\text{In}_{12}$  cage (dimension  $\sim 0.9 \text{ nm}$ ) and the  $\text{In}_{24}$  cage ( $\sim 2.5 \text{ nm}$ ) (Figure 1c) by 12 BTCs serves to partition the pore space of the large sodalite cage into multiple domains with the pore radius in the range of  $4.00\text{--}1.68 \text{ \AA}$  (volume:  $268\text{--}19.9 \text{ \AA}^3$ ) (Table S2).<sup>15</sup> Even with the small  $\text{In}_{12}$  cage within the  $\text{In}_{24}$  cage and the BTC interconnectors between  $\text{In}_{12}$  and  $\text{In}_{24}$  cages, CPM-5 still possesses a relatively large guest-accessible volume of  $8141 \text{ \AA}^3$  per unit cell (47.9% of the total unit cell volume). The formation of the cage-within-cage structure is related to two distinctly different  $\text{In}^{3+}$  configurations: a monomeric four-connected  $[\text{In}(\text{O}_2\text{CR})_4]^-$  site and trimeric  $[\text{In}_3(\text{O})(\text{O}_2\text{CR})_6(\text{H}_2\text{O})_3]^+$  clusters. Currently, the design and synthesis of single metal-based zeolite-like MOFs or MBB-based (MBB = molecular building block) porous MOFs are two active areas. In comparison, MOFs that integrate both single-metal and metal-cluster building units are less well-known and represent a fruitful route for the design of novel porous materials. In CPM-5, both single metal  $\{[\text{In}(\text{O}_2\text{CR})_4]\}$  units and the trimeric  $\{[\text{In}_3(\text{O})(\text{O}_2\text{CR})_6(\text{H}_2\text{O})_3]\}$  MBBs are present. Since the  $\text{In}/\text{COO}^-$  ratio in the structure differs greatly depending on whether the indium sites exist in the monomeric form or trimeric forms, a systematic synthetic exploration of the  $\text{In}/\text{COO}^-$  ratio represents a viable strategy for the selection of the desired  $\text{In}$  form, even if the  $\text{In}/$

$\text{COO}^-$  ratio in the crystal structures does not necessarily correspond to a particular range of  $\text{In}/\text{COO}^-$  ratios in the synthesis mixture. It is of particular interest that the outer cage made from single metal  $\{[\text{In}(\text{O}_2\text{CR})_4]\}$  units is negatively charged whereas the inner cage made from trimeric  $\{[\text{In}_3(\text{O})(\text{O}_2\text{CR})_6(\text{H}_2\text{O})_3]\}$  MBBs is positively charged, leading to an electric field within the shell region between  $\text{In}_{24}$  and  $\text{In}_{12}$  cages. In addition to the pore space partitioning and the electric field effect associated with the cage-within-cage architecture, CPM-5 integrates another desirable feature, open metal sites. Attached to each indium ion of the inner  $\text{In}_{12}$  cage (67% of all indium sites in CPM-5) is a dangling water ligand which upon removal serves to generate open  $\text{In}^{3+}$  sites, as supported by IR spectra of the CPM-5 sample before and after degassing (Figure S4).

A large quantity of pure CPM-5 (gram-scale) can be readily prepared. Powder X-ray diffraction (PXRD) indicates CPM-5 is stable in water at room temperature and remains highly crystalline even after being in boiling water for 8 h (Figure S5). Furthermore, CPM-5 is stable photochemically and retains its crystallinity after exposure to strong UV radiations for 10 h (Figure S6). Thermogravimetric analysis of CPM-5 shows that the removal of solvent molecules occurs in the temperature range of  $40\text{--}230 \text{ }^\circ\text{C}$  and no further weight loss up to  $300 \text{ }^\circ\text{C}$  (Figure S7). PXRD further confirms that the desolvated sample retains its crystallinity up to about  $320 \text{ }^\circ\text{C}$  (Figure S8).

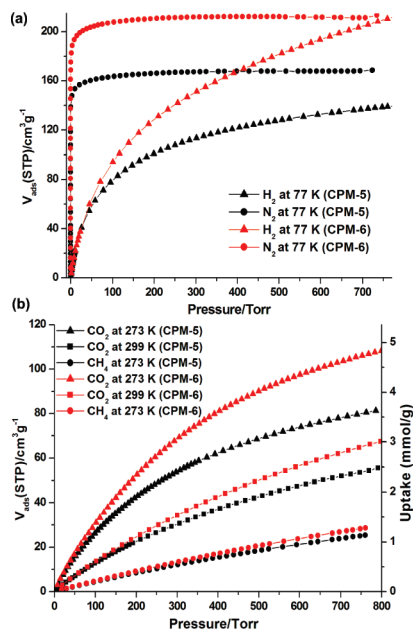


**Figure 3.** (a)  $\text{N}_2$  and  $\text{H}_2$  adsorption isotherms of CPM-5 and CPM-6. (b)  $\text{CO}_2$  and  $\text{CH}_4$  adsorption isotherms of CPM-5 and CPM-6.

Interestingly, CPM-5', a tetragonal variation of cubic CPM-5, can be prepared in the presence of 4,4'-bipyridine (Figure S9). The only difference between CPM-5 and CPM-5' is in the coordination of the monomeric indium site on the outer  $\text{In}_{24}$  cage. In CPM-5,  $\text{H}_2\text{O}$  only attaches to the inner  $\text{In}_{12}$  cage whereas, in CPM-5', two-thirds of  $\text{In}^{3+}$  sites on the  $\text{In}_{24}$  cage are also bonded to  $\text{H}_2\text{O}$  (in addition to  $\text{H}_2\text{O}$  on the  $\text{In}_{12}$  cage). PXRD shows that CPM-5' can be converted to CPM-5 after  $\text{H}_2\text{O}$  on the  $\text{In}_{24}$  cage is removed at  $230 \text{ }^\circ\text{C}$  (Figure S10).

Hydrothermal, thermal, and photochemical stability, coupled with open indium sites, pore space partitioning, and favorable charge separation in CPM-5 render it a good candidate for the study of gas sorption properties. The measurements ( $\text{N}_2$ ,  $\text{H}_2$ ,  $\text{CH}_4$ , and  $\text{CO}_2$ )

were performed on a Micromeritics ASAP 2020 surface-area and pore-size analyzer. No sample activation was applied, and the as-synthesized sample was directly degassed at 230 °C for 48 h under vacuum prior to the measurement. CPM-5 exhibits a type I adsorption isotherm typical of materials of permanent microporosity (Figure 3a). The Langmuir and BET surface areas were 733 and 580 m<sup>2</sup>/g, respectively. A micropore volume of 0.258 cm<sup>3</sup>/g (using Horvath–Kawazoe method) and the median pore size of 4.89 Å were also calculated. The small pore size is clearly the effect of the pore size partition resulting from the unique In<sub>12</sub>@In<sub>24</sub> topology.

CPM-5 exhibits a very high CO<sub>2</sub> uptake capacity of 81.3 cm<sup>3</sup>/g (91.3 L/L) at 273 K and 1 atm (Figure 3b). At room temperature (299 K) and 1 atm, CPM-5 has a CO<sub>2</sub> uptake of 54.5 cm<sup>3</sup>/g (61.2 L/L). It is worth noting that even though numerous MOF structures have been reported, few exhibit a CO<sub>2</sub> uptake of more than 60 L/L at 298 K and 1 atm.<sup>4c,16,17</sup> Clearly, the unique structural factors of CPM-5 described above contribute significantly to its high CO<sub>2</sub> uptake. For H<sub>2</sub> gas, the adsorption isotherms revealed that CPM-5 can adsorb 139.2 cm<sup>3</sup>/g of H<sub>2</sub> (1.24 wt %) at 77 K and 1 atm.

To further improve the gas uptake capacity, we also varied the size of extraframework organic cations and prepared an isostructural compound CPM-6 with smaller organic cations (CH<sub>3</sub>NH<sub>3</sub><sup>+</sup>, Figure S11). As expected, CPM-6 exhibits significantly improved gas sorption properties. While the improvement in the surface area is moderate (the Langmuir and BET surface areas of CPM-6 are 931 and 596 m<sup>2</sup>/g, respectively), the CO<sub>2</sub> and H<sub>2</sub> uptake capacities of CPM-6 are remarkably enhanced (for CO<sub>2</sub> at 1 atm: 106.7 cm<sup>3</sup>/g (119.8 L/L) at 273 K and 65 cm<sup>3</sup>/g (73 L/L) at 299 K; for H<sub>2</sub> at 1 atm: 210.6 cm<sup>3</sup>/g (1.88 wt %) at 77 K). In comparison, the adsorption of CH<sub>4</sub> gas on both CPM-5 and CPM-6 are markedly lower than that of CO<sub>2</sub>. At 273 K, the CO<sub>2</sub>/CH<sub>4</sub> ratios of uptake are ca. 7.5–3.2 between 0.01 and 1 bar.

In conclusion, the integration of negatively charged single-metal building blocks {In(CO<sub>2</sub>)<sub>4</sub>} and positively charged trimeric clusters {In<sub>3</sub>O} leads to an exceptional porous material in which the large In<sub>24</sub> sodalite cage encapsulates and interconnects a small In<sub>12</sub> cage laden with open In<sup>3+</sup> sites. The cage-within-cage architecture partitions the pore space into small charge-separated domains that are among key desirable features needed for enhanced gas sorption through a better size match and stronger charged-induced forces. These integrated structural features (i.e., open metal sites, pore size partition, and electric field) contribute to a very high CO<sub>2</sub> uptake capacity. Furthermore, the material exhibits a high hydrothermal, thermal, and photochemical stability.

**Acknowledgment.** We thank the support of this work by the NSF (X.B., DMR-0846958) and DOE (P.F., ER46631; DE-SC0002235). X.B. is a Henry Dreyfus Teacher Scholar.

**Supporting Information Available:** Experimental details, TGA, XRPD, EA, IR, and additional figures. This material is available free of charge via the Internet at <http://pubs.acs.org>.

## References

- (1) (a) Xiao, B.; Byrne, P. J.; Wheatley, P. S.; Wragg, D. S.; Zhao, X.; Fletcher, A. J.; Thomas, K. M.; Peters, L.; Evans, J. S. O.; Warren, J. E.; Zhou, W.; Morris, R. E. *Nat. Chem.* **2009**, *1*, 289. (b) Phan, A.; Doonan, C. J.; Uriberomo, F. J.; Knobler, C. B.; O'Keefe, M.; Yaghi, O. M. *Acc. Chem. Res.* **2010**, *43*, 58–67. (c) Tanaka, D.; Henke, A.; Albrecht, K.; Moeller, M.; Nakagawa, K.; Kitagawa, S.; Groll, J. *Nat. Chem.* **2010**, *2*, 410–416. (d) Ma, L.; Falkowski, J. M.; Abney, C.; Lin, W. *Nat. Chem.* **2010**, *2*, 838–846.
- (2) (a) Xiang, S.; Zhou, W.; Gallegos, J. M.; Liu, Y.; Chen, B. L. *J. Am. Chem. Soc.* **2009**, *131*, 12415–12419. (b) Li, K.; Olson, D. H.; Seidel, J.; Emge, T. J.; Gong, H.; Zeng, H.; Li, J. *J. Am. Chem. Soc.* **2009**, *131*, 10368–10369. (c) Lee, Y.; Farha, O. K.; Roberts, J.; Scheidt, K. A.; Nguyen, S. T.; Hupp, J. T. *Chem. Soc. Rev.* **2009**, *38*, 1450–1459.
- (3) (a) Zhao, D.; Yuan, D.; Zhou, H. C. *Energy Environ. Sci.* **2008**, *1*, 222–235. (b) Sava, D. F.; Kravtsov, V. C.; Eckert, J.; Eubank, J. F.; Nouar, F.; Eddaoudi, M. *J. Am. Chem. Soc.* **2009**, *131*, 2864–10396. (c) Zheng, S.; Wu, T.; Zhang, J.; Chow, M.; Nieto, R. A.; Feng, P.; Bu, X. *Angew. Chem., Int. Ed.* **2010**, *49*, 5362–5366. (d) Hu, Y. H.; Zhang, L. *Adv. Mater.* **2010**, *22*, E117–E130.
- (4) (a) An, J.; Fiorella, R. P.; Geib, S. J.; Rosi, N. L. *J. Am. Chem. Soc.* **2009**, *131*, 8401–8403. (b) An, J.; Rosi, N. L. *J. Am. Chem. Soc.* **2010**, *132*, 5578–5579. (c) Debatin, F.; Thomas, A.; Kelling, A.; Hedin, N.; Bacsik, Z.; Senkowska, I.; Kaskel, S.; Junginger, M.; Müller, H.; Schilde, U.; Jäger, C.; Friedrich, A.; Holdt, H. *J. Angew. Chem., Int. Ed.* **2010**, *49*, 1258–1262.
- (5) (a) Morris, R. E.; Wheatley, P. S. *Angew. Chem., Int. Ed.* **2008**, *47*, 4966–4981. (b) Demessence, A.; D'Alessandro, D. M.; Foo, M. L.; Long, J. R. *J. Am. Chem. Soc.* **2009**, *131*, 8784–8786. (c) Banerjee, R.; Furukawa, H.; Britt, D.; Knobler, C.; O'Keefe, M.; Yaghi, O. M. *J. Am. Chem. Soc.* **2009**, *131*, 3875–3877.
- (6) (a) Férey, G. *Chem. Soc. Rev.* **2008**, *37*, 191–214. (b) Yuan, D.; Zhao, D.; Sun, D.; Zhou, H. C. *Angew. Chem., Int. Ed.* **2010**, *49*, 5357–5361. (c) Deng, H.; Doonan, C. J.; Furukawa, H.; Ferreira, R. B.; Towne, J.; Knobler, C. B.; Wang, B.; Yaghi, O. M. *Science* **2010**, *327*, 846–850.
- (7) (a) Koh, K.; Wong-Foy, A. G.; Matzger, A. J. *J. Am. Chem. Soc.* **2009**, *131*, 4184–4185. (b) Zhao, D.; Yuan, D.; Sun, D.; Zhou, H. C. *J. Am. Chem. Soc.* **2009**, *131*, 9186–9188. (c) Furukawa, H.; Ko, N.; Go, Y. B.; Aratani, N.; Choi, S. B.; Choi, E.; Yazaydin, A. O.; Snurr, R. Q.; O'Keefe, M.; Kim, J.; Yaghi, O. M. *Science* **2010**, *329*, 427–428.
- (8) (a) Murray, L. J.; Dinca, M.; Long, J. R. *Chem. Soc. Rev.* **2009**, *38*, 1294–1314. (b) Han, S. S.; Mendoza-Cortés, J. L.; Goddard, W. A., III. *Chem. Soc. Rev.* **2009**, *38*, 1460–1476. (c) Xiang, S.; Zhou, W.; Zhang, Z.; Green, M. A.; Liu, Y.; Chen, B. *Angew. Chem., Int. Ed.* **2010**, *49*, 4615–4618.
- (9) (a) Sava, D. F.; Kravtsov, V. C.; Eckert, J.; Eubank, J. F.; Nouar, F.; Eddaoudi, M. *J. Am. Chem. Soc.* **2009**, *131*, 10394–10396. (b) Ma, L.; Lin, W. *Angew. Chem., Int. Ed.* **2009**, *48*, 3637–3640. (c) Lin, J. B.; Zhang, J. P.; Chen, X. M. *J. Am. Chem. Soc.* **2010**, *132*, 6654–6656. (d) Farha, O. K.; Malliakas, C. D.; Kanatzidis, M. G.; Hupp, J. T. *J. Am. Chem. Soc.* **2010**, *132*, 950–952.
- (10) (a) Dincă, M.; Long, J. R. *Angew. Chem., Int. Ed.* **2008**, *47*, 6766–6779. (b) Himsl, D.; Wallacher, D.; Hartmann, M. *Angew. Chem., Int. Ed.* **2009**, *48*, 4639–4642. (c) Mulfort, K. L.; Farha, O. K.; Stern, C. L.; Sarjeant, A. A.; Hupp, J. T. *J. Am. Chem. Soc.* **2009**, *131*, 3866–3868. (d) Ma, L.; Jin, A.; Xie, Z.; Lin, W. *Angew. Chem., Int. Ed.* **2009**, *48*, 9905–9908.
- (11) (a) Dören, T.; Baeb, Y. S.; Snurr, R. Q. *Chem. Soc. Rev.* **2009**, *38*, 1237–1247. (b) Mavrandonakis, A.; Klontzas, E.; Tylilanakis, E.; Froudakis, G. E. *J. Am. Chem. Soc.* **2009**, *131*, 13410–13414. (c) Higuchi, M.; Tanaka, D.; Horike, S.; Sakamoto, H.; Nakamura, K.; Takashima, Y.; Hijikata, Y.; Yanai, N.; Kim, J.; Kato, K.; Kubota, Y.; Takata, M.; Kitagawa, S. *J. Am. Chem. Soc.* **2009**, *131*, 10336–10337. (d) Yang, S.; Lin, X.; Blake, A. J.; Walker, G.; Hubberstey, P.; Champness, N. R.; Schröder, M. *Nat. Chem.* **2009**, *1*, 487–493.
- (12) (a) Barea, E.; Navarro, J. A. R.; Salas, J. M.; Masciocchi, N.; Galli, S.; Sironi, A. *J. Am. Chem. Soc.* **2004**, *126*, 3014–3015. (b) Liu, Y.; Kravtsov, V. C.; Larsena, R.; Eddaoudi, M. *Chem. Commun.* **2006**, 1488–1490. (c) Galli, S.; Masciocchi, N.; Tagliabue, G.; Sironi, A.; Navarro, J. A. R.; Salas, J. M.; Mendez-Liñan, L.; Domingo, M.; Perez-Mendoza, M.; Barea, E. *Chem.–Eur. J.* **2008**, *14*, 9890–9901.
- (13) (a) Liu, Y.; Eubank, J. F.; Cairns, A. J.; Eckert, J.; Kravtsov, V. C.; Luebke, R.; Eddaoudi, M. *Angew. Chem., Int. Ed.* **2007**, *46*, 3278–3283. (b) Tranchmontagne, D. J.; Ni, Z.; O'Keefe, M.; Yaghi, O. M. *Angew. Chem., Int. Ed.* **2008**, *47*, 5136–5147. (c) Zhao, D.; Yuan, D.; Sun, D.; Zhou, H. C. *J. Am. Chem. Soc.* **2009**, *131*, 9186–9188.
- (14) (a) Chen, B.; Ockwig, N. W.; Millward, A. R.; Contreras, D. S.; Yaghi, O. M. *Angew. Chem., Int. Ed.* **2005**, *44*, 4745–4749. (b) Sava, D. F.; Kravtsov, V. C.; Nouar, F.; Wojtas, L.; Eubank, J. F.; Eddaoudi, M. *J. Am. Chem. Soc.* **2008**, *130*, 3766–3770. (c) Yan, Y.; Telepeni, I.; Yang, S.; Lin, X.; Kockelmann, W.; Dailly, A.; Blake, A. J.; Lewis, W.; Walker, G. S.; Allan, D. R.; Barnett, S. A.; Champness, N. R.; Schröder, M. *J. Am. Chem. Soc.* **2010**, *132*, 4092–4094.
- (15) PLATON VOIDS probe diameter 1.2 Å; Spek, A. L. *J. Appl. Crystallogr.* **2003**, *36*, 7–13.
- (16) Banerjee, R.; Phan, A.; Wang, B.; Knobler, C.; Furukawa, H.; O'Keefe, M.; Yaghi, O. M. *Science* **2008**, *319*, 939.
- (17) Alessandri, D. M. D.; Smit, B.; Long, J. R. *Angew. Chem., Int. Ed.* **2010**, *49*, 6058–6082.

JA106903P